

## Article

# Standardizing the Ignition Delay Time Measurements of Rapid Compression Machine: An Inverse Application of the Livengood–Wu Integral Method

Zhonghao Zhao <sup>1,2</sup>  and Yingtao Wu <sup>1,2,\*</sup>

<sup>1</sup> Petroleum, Oil & Lubricants Department in Army Logistics Academy of PLA, Chongqing 401311, China; zhaozhonghao9302@163.com

<sup>2</sup> State Key Laboratory of Multiphase Flow in Power Engineering, Xi'an Jiaotong University, Xi'an 710049, China

\* Correspondence: wuyingtao@xjtu.edu.cn; Tel.: +86-29-8266-5075; Fax: +86-29-8266-8789

**Abstract:** The rapid compression machine measures ignition delay time at high pressures and low to intermediate temperatures. However, unavoidable facility effects, such as compression and heat loss, shift the measurements away from ideal (adiabatic and constant volume) values to varying extents. Consequently, the ignition delay times measured by different facilities can be in large deviations, especially for fuel mixtures without negative temperature coefficient behavior. To address this issue, this work proposes a standardization algorithm that correlates the measurements to the ideal ignition delay times. The algorithm applies the Livengood–Wu integral method inversely and adopts a Bayesian approach to optimize the correlation parameters. The ignition delay times of an ethanol mixture under distinct facility effects were further used to test the performance of this algorithm. The results show that the dispersed ignition delay times can be effectively standardized within 20%, facilitating the direct comparison of measurements from different facilities. By setting a proper residual target of the algorithm, reasonable standardization accuracy can be achieved. This method enables a significantly easier interpretation of the rapid compression machine experimental data and can be broadly applied to any fuel mixtures exhibiting single-stage ignition characteristics.



Academic Editor: Constantine D. Rakopoulos

Received: 11 November 2024

Revised: 24 December 2024

Accepted: 2 January 2025

Published: 3 January 2025

**Citation:** Zhao, Z.; Wu, Y.

Standardizing the Ignition Delay Time Measurements of Rapid Compression Machine: An Inverse Application of the Livengood–Wu Integral Method. *Energies* **2025**, *18*, 165. <https://doi.org/10.3390/en18010165>

**Copyright:** © 2025 by the authors.

Licensee MDPI, Basel, Switzerland.

This article is an open access article distributed under the terms and conditions of the Creative Commons Attribution (CC BY) license (<https://creativecommons.org/licenses/by/4.0/>).

**Keywords:** rapid compression machine; ignition delay time; facility effect; standardization; inverse Livengood–Wu integral

## 1. Introduction

Ignition delay time (IDT) [1], which characterizes the global reactivity of a combustible mixture, is a crucial parameter in combustion research. While the definitions of IDT may vary among facilities, it typically represents the induction time from thermal stimulus to a violent chemical reaction. Modern engine design requires precise control of IDT to achieve high thermal efficiency, avoid knock and instability, and reduce pollutant emissions [2,3]. Therefore, IDT is also an important parameter for evaluating the feasibility of alternative fuels.

IDT is typically measured by shock tube (ST), rapid compression machine (RCM) and constant volume bomb (CVB), each designed for different measurement time scales and temperature ranges [4,5]. Specifically, ST is suitable for measuring IDTs within the range of a few milliseconds at high temperatures [6]. Limited by the time scale of heating the injected fuel mixtures, CVB is generally used to measure IDTs from  $10^{-1}$  s to  $10^1$  s and is

more suitable for determining the autoignition limits [7]. Complementarily, RCM achieves low to intermediate temperatures and high pressures through fast piston compression and is effective in measuring IDTs from  $10^0$  to  $10^2$  milliseconds [4].

The IDTs obtained from ST and RCM are often used to validate the chemical kinetic mechanism of fuels [8]. However, compared to that of ST, the thermal condition of RCM is less ideal, and its measurements are more intended to be affected by the facility effects [9]. IDTs measured by different STs can usually be compared directly [10], while the measurements of different RCMs cannot [9,11,12]. Two typical pressure traces from ST [13] and RCM [14], respectively, are compared with normalized time, as shown in Figure 1. The thermal condition in ST is built up almost instantly through the compression of a shock wave. In contrast, the compression process in RCM is limited by the piston movement, and noteworthy chemical reactions can take place in this process, shortening the IDT measurement, especially for conditions with higher reactivities. Furthermore, due to the longer time scale of the RCM measurement, the heat transfer between the gas mixture and the chamber wall cannot be neglected, which results in a gradual pressure drop before the ignition, as shown in the RCM nonreactive measurement (replacing  $O_2$  with  $N_2$  in the mixture) in Figure 1. The heat loss tends to prolong the IDT measurement, especially for conditions with lower reactivities. As a result, RCMs with different geometries and piston movement designs may have distinct measurements of IDTs, even though all of them are “accurate” in the modeling [4,9].

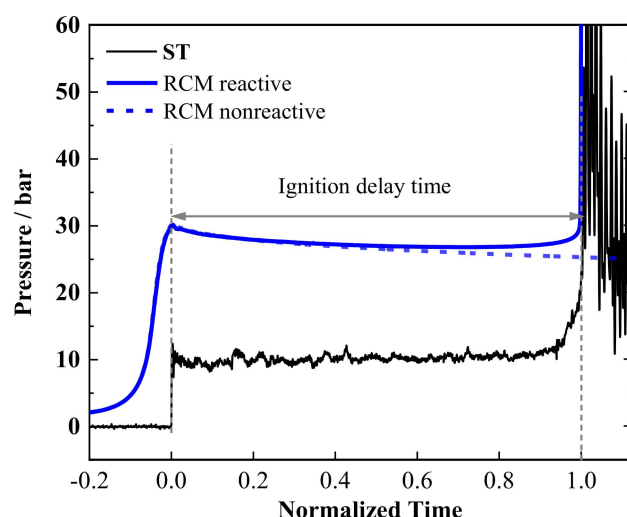


**Figure 1.** Comparison of the pressure measurements between ST [13] and RCM [14].

To accommodate the facility effect of the RCM measurement, the volume tabulation method [15,16] is usually adopted in the zero-dimensional (0D) kinetic simulation. The volume profile is derived from the nonreactive pressure trace using Equations (1) and (2) under the assumption of the “adiabatic core” theory [17].

$$\int_{T_0}^T \frac{\gamma}{\gamma - 1} \frac{dT}{T} = \ln\left(\frac{p}{p_0}\right) \quad (1)$$

$$\int_{T_0}^T \frac{1}{\gamma - 1} \frac{dT}{T} = \ln\left(\frac{V}{V_0}\right) \quad (2)$$

where  $T_0$ ,  $p_0$ , and  $V_0$  are the initial temperature, pressure and volume, respectively;  $T$ ,  $p$ , and  $V$  are the temperature, pressure, and volume, respectively, at any time; and  $\gamma$  is the temperature-dependent specific heat ratio of the mixture.

With the help of the volume tabulation method, the “accurate” RCM measurements should achieve equal agreement with the model simulation results. Despite this, the RCM experiments still require rigorous specification of the initial and boundary conditions, i.e., heat loss characteristics. Using simple characteristic parameters, such as compressed temperature and pressure, as the basis to evaluate the experimental results of different RCMs remains a challenge, as illustrated in the international RCM workshop [4]. To find a common ground for RCM experiments, Preußker et al. [9] modified their RCM to unconventional operation conditions, including variations of the piston compression from creep to abrupt stopping, usage of different piston crevice geometries, and altered dead volume of the combustion chamber. By adopting the volume tabulation approach, 98% of the IDT measurements with altered facility effects can be predicted within  $\pm 25\%$  using one single mechanism. Büttgen et al. [12] investigated the IDTs of ethanol obtained from five independent RCMs. As expected, the raw measurements of these RCMs show notable differences at the same thermal conditions. With the facility effects considered through the volume tabulation approach, the chemical kinetic model can predict all experimental data within the uncertainty. Their work put emphasis on repeating experimental data using various facilities.

Another suitable approach to predicting the IDT under transient thermal environments is the Livengood–Wu (L–W) integral method [18], which has been effectively applied in engine knock prediction [19–24], as well as the onset of ignition in compression ignition engines and homogeneous charged compression ignition engines [20,25,26]. A general formulation of the L–W integral is written as Equation (3), where  $x(t)$  represents an ignition carrier and can only be accumulated up to its critical value  $x_c$ . The integration equals 1 at the time of ignition.

$$\frac{x(t)}{x_c} = \int_0^t \frac{1}{\tau} dt \quad (3)$$

Briefly, the L–W integral method assumes the ignition carrier reaches its critical concentration by summing up the carriers formed at each quasi-steady state, in which the production rate of the carriers is simplified as  $1/\tau$ . Although the L–W method was developed by assuming a zeroth order kinetics of the system, Khaled et al. [27], Pan [28] and Miyoshi [29] further theoretically rationalized the validity of this method for any global order kinetics.

Since the L–W integral method can predict the IDTs under transient thermal conditions using the IDTs at ideal steady states, it would be worthy to test the inverse application of this method, namely, to predict the IDTs at ideal conditions based on the autoignition profiles measured under varying thermal conditions. Reyes et al. [5] adopted an inverse L–W method to obtain the analytical expressions of IDT from the autoignition timing measured in a CVB. The work studied fuels like *n*-heptane while assuming a simple Arrhenius IDT expression. Since the two-stage heat release and negative temperature coefficient (NTC) characteristics of *n*-heptane were not considered in their method, the correlated IDTs still showed large deviations with the other measurements. Tao et al. [30] incorporated the genetic algorithm in the inverse L–W method to interpret the IDTs measured in a high repetition rate miniature shock tube. Their optimized solutions on the IDT correlation showed a very good agreement with the reference data, demonstrating the feasibility of the inverse use of the L–W integral method at high-temperature conditions.

For fuels with two-stage ignition and NTC behaviors, such as *n*-heptane and *iso*-octane, the agreement of the IDT measurements among different RCMs is generally acceptable [4,31]. In contrast, fuels with low low-temperature reactivity (L-fuels), like ethanol and methane, exhibited much larger deviations in IDT measurements among different RCMs [9,11]. To our knowledge, no reliable method exists to standardize the IDTs of the L-fuels, despite the fact that their autoignition characteristics (single-stage and no NTC) are well suited for the inverse L–W integral method. To interpret the RCM data, the volume tabulation method remains the most prevalent approach to date. This indirect interpretation of RCM experimental data, though it performs well in the model validation, is time-consuming and can be influenced by the uncertainties in the chemical kinetic model. Shah et al. [32] also pointed out that uncertainties in the kinetic model can be significantly amplified for model-based control of ignition timing in advanced compression ignition engines. This motivates our work to develop a method that can interpret the RCM measurement without involving complex kinetic modeling and enable the direct comparison of the IDTs from different facilities.

In this work, we propose an algorithm that combines the inverse L–W integral method with the Bayesian optimization approach [24] to standardize the IDTs under different facility effects. The standardization procedure is introduced first in the following sections. Autoignitions of an ethanol mixture under distinct facility effects are then used to test the forward predictions of the L–W integral method. Sensitivity analyses of the IDT correlation parameters are conducted to improve the efficiency of hyperparameter optimization. Finally, IDT correlations obtained from the inverse L–W integral method at various residual levels are presented, and their performance in terms of IDT standardization accuracy is discussed.

## 2. Standardization Method Procedure

The standardization procedure for the IDTs obtained from RCM is shown in Figure 2, which mainly includes input data preparation, IDT correlation (parameter fit), and hyperparameter optimization (residuals and GP optimization).

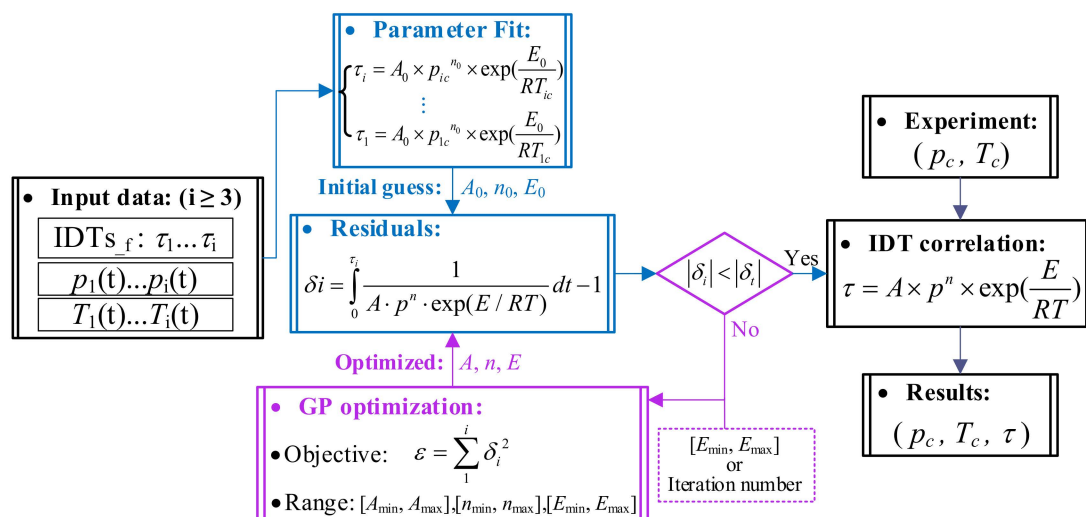


**Figure 2.** Standardization procedure for the IDTs from RCM.

### 2.1. Input Data Preparation

To calculate the IDT at each quasi-steady state, the input data should include pressure profiles, temperature profiles and the corresponding global IDTs\_f (IDTs affected by facility effects). In RCM experiments, the pressure in the combustion chamber can be directly

measured by a transducer, while the temperature profiles of the core region are derived from the pressure using Equation (1). A properly designed RCM piston is a prerequisite for the validity of the “adiabatic core” theory [17], thereby ensuring the accuracy of the temperature profiles.

In this study, we adopt three types of volume profiles, mimicking different facility effects, to generate input data, as shown in Figure 3. Inputs-1 and inputs-2 are from the RCM at Xi’an Jiaotong University [11,33], while inputs-3 is from the RCM at the University of Galway. [34]. Inputs-1 to inputs-3 were modified to have the same compression ratio. The inputs-1 has the largest volume expansion rate after the end of compression (EOC), presenting the most severe heat loss, which would typically occur with a short combustion chamber. Inputs-2 follows the same compression process as inputs-1 but with the least heat loss. The compression process of inputs-3 is much faster, and its heat loss is between inputs-1 and inputs-2.

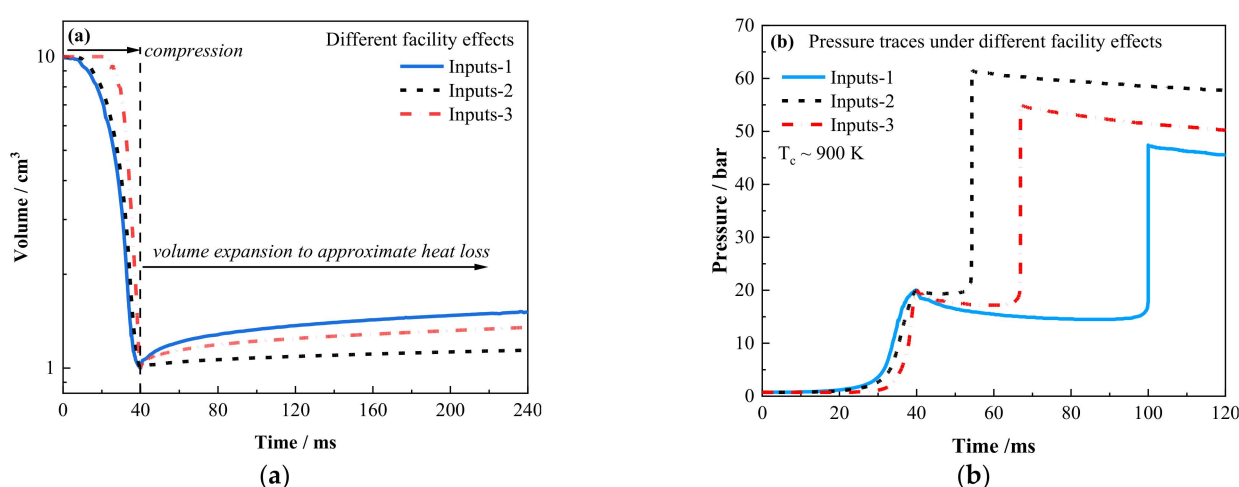


**Figure 3.** (a) The input volume profiles mimicking different facility effects. (b) Simulated pressure traces at  $T_c \sim 900$  K under different facility effects.

An ethanol chemical kinetic model extracted from NUIGMech1.1 [34] was adopted in the kinetic simulation using Cantera. The ethanol sub-mech in NUIGMech1.1 has been sufficiently validated against a wide range of experimental data, including IDTs from ST [35] and RCM [36], speciation in a Jet-stirred reactor [37] and laminar flame speed [38]. Details of the validation can be found in the mechanism website of Galway (<https://www.universityofgalway.ie/media/researchcentres/combustionchemistrycentre/files/C2.pdf>, accessed on 1 January 2025). With the constrained volume profile, the temperature and pressure profiles in the reactor are determined by solving the ideal gas law and energy equation. IDT is defined as the time interval between end of compression and the instant of maximum  $dp/dt$ . Examples of the autoignition pressure traces for the ethanol mixture (3.72% C<sub>2</sub>H<sub>5</sub>OH, 11.17% O<sub>2</sub> and 85.11% diluents) at  $T_c \sim 900$  K (temperature at the end of compression) are shown in Figure 3b. Inputs-1 has the longest IDT (60 ms) due to the most severe heat loss. With less heat loss in inputs-2 and inputs-3, their IDTs decrease to 14.1 ms and 26.8 ms, respectively.

By adjusting  $T_0$  prior to each simulation,  $T_c$  was varied accordingly, and the IDTs for each input set were maintained within the typical RCM measurement range (5–200 ms), as shown in Figure 4. For each set of simulations,  $p_0$  was slightly adjusted to ensure that  $p_c$  remained approximately 20 bar. Temperature and pressure profiles required by the algorithm were obtained from the Cantera simulation results and stored in csv files. The global IDTs\_f was attached as the label of the corresponding csv file.

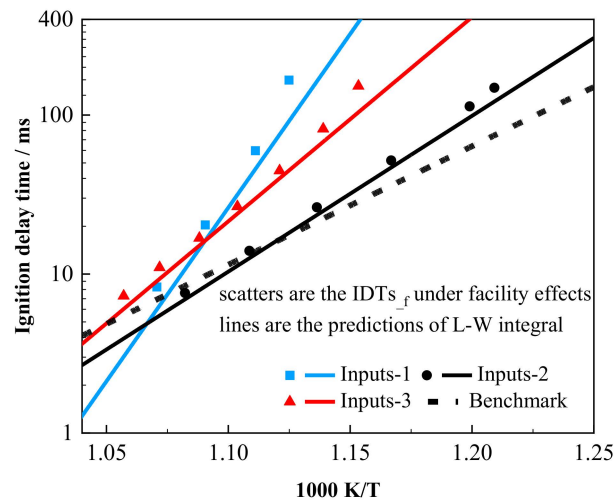


**Figure 4.** The IDTs under different facility effects and the predictions of the L–W integral.

### 2.2. IDT Correlation

The IDTs can generally be correlated using an Arrhenius expression at both high [26] and low temperatures [20] (outside of the NTC region), as shown in Equation (4).

$$\tau = A \times \prod x_i^{a_i} \times p^n \times \exp\left(\frac{E}{RT}\right) \quad (4)$$

where  $\tau$  is the IDT;  $x_i$  is the concentration of the species;  $R$  is the gas constant;  $A$ ,  $a_i$ ,  $n$  and  $E$  are the fitted parameters. Specially,  $E$  is also called the activation energy of the mixture. For the ethanol mixture, the IDTs show a typical Arrhenius temperature dependence and can be simplified as Equation (5) when the composition is fixed.

$$\tau = A \times p^n \times \exp\left(\frac{E}{RT}\right) \quad (5)$$

where  $\tau$  is in milliseconds,  $p$  is in bar,  $T$  is in K, and  $R$  is in  $\text{J/mol}\cdot\text{K}^{-1}$  in this work.

The IDTs<sub>f</sub> are firstly used to fit the three parameters of the Arrhenius expression using the least squares method, obtaining an initial guess ( $A_0$ ,  $n_0$  and  $E_0$ ) of the IDT correlation. The algorithm can then enter into the next part: optimizing these parameters for the ideal IDT<sub>cv</sub> correlation.

### 2.3. Hyperparameter Optimization Algorithm

At least three input files of each set are required for the hyperparameter optimization since the target IDT correlation, Equation (5), contains three unknown parameters, i.e.,  $A$ ,  $n$  and  $E$ .  $A_0$ ,  $n_0$  and  $E_0$  obtained from last step are adopted in the forward L–W integral from time zero to the ignition time (compression time + IDT<sub>f</sub>). Residual ( $\delta$ ) of the current optimization result is defined as Equation (6), where 1 represents ignition in the L–W integral method. A negative  $\delta$  therefore indicates the L–W integral does not reach 1 at the time of ignition, which means the current IDT correlation is slower. Conversely, a positive  $\delta$  indicates a faster IDT correlation.

$$\delta_i = \int_0^{\tau_i} \frac{1}{A \cdot p^n \cdot \exp(E/RT)} dt - 1 \quad (6)$$

If all  $\delta_i$  meet the target residual ( $\delta_i$ ), these three parameters will then constitute the target correlation expression.

Without extensive optimization,  $|\delta_i|$  can be very large. To address this, we adopt a Bayesian optimization approach [39] to optimize the hyperparameters of the Arrhenius expression. Within this framework, the Gaussian process optimization was used as the specific implementation, which minimizes the objective function ( $\varepsilon = \sum_1^i \delta_i^2$ ) using a Gaussian process (GP). If  $\delta_i$  cannot meet the requirement after one cycle of optimization, ranges of the hyperparameters can be gradually narrowed down based on previous best estimations or increasing the iteration number of the GP process. With the optimized A, n and E, the Arrhenius expression can then be used to correlate the  $IDTs_{-f}$  to those at the ideal constant volume and adiabatic conditions ( $IDTs_{-cv}$ ): the measured  $p_c$  and  $T_c$  from the experiments were substituted for  $p$  and  $T$  in the correlation, respectively.

### 3. Results and Discussion

This work emphasizes the performance of the standardization method; therefore, constant volume and adiabatic simulation results using the chemical kinetic model are adopted as the ground truth for quantitative evaluation.

#### 3.1. Forward Prediction of the L–W Integral

Before applying the inverse method of the L–W integral, we first test the predictive ability of the forward L–W integral method. As shown in Figure 4, the IDTs under different facility effects (inputs-1 to inputs-3) exhibit significant deviations. However, since all the scatter data were calculated using the same chemical kinetic model, these “measurements” are chemically accurate, and any discrepancies arise solely from the facility effects. The dashed line is the adiabatic constant volume simulation result, and its IDTs are given by Equation (7).

$$\tau = 1.077 \times 10^{-6} \times p^{(-9.017 \times 10^{-1})} \times \exp\left(1.427 \times 10^5 / T\right) \quad (7)$$

Using Equation (7), the  $IDTs_{-f}$  under varying thermal conditions of inputs-1 to inputs-3 are predicted as the solid lines in Figure 4. Generally, the L–W integral predictions agree well with the  $IDTs_{-f}$ . The largest deviation occurs at 889 K of the inputs-1, which is around 45.7%. For inputs-2 and inputs-3, the largest deviations also occur at the lowest temperatures, which are around 18.5% and 30.9%, respectively.

To quantify the overall agreement of the L–W integral prediction under different inputs cases, an Average Relative Deviation (ARD) is defined by Equation (8), where n represents the number of cases for each input set.  $IDT_i$  is the individual IDT prediction using the L–W integral, while  $IDT_{i,real}$  is the IDT calculated through chemical kinetic simulation. As shown in Table 1, the ARD exhibits a positive correlation with the heat loss rate of different inputs. In other words, errors of the L–W integral predictions are larger under conditions with more severe heat loss.

$$ARD = \frac{\sqrt{\sum_{i=1}^n \left(\frac{IDT_i - IDT_{i,real}}{IDT_{i,real}}\right)^2}}{n} \times 100\% \quad (8)$$

**Table 1.** ARD for inputs-1 to inputs-3.

Inputs	ARD/%
1	15.4
2	5.1
3	6.6

The L–W integral predictions are all slightly lower than the  $IDT_{s_f}$ . To figure out the possible explanation, instants of the L–W integral equal to 1 ( $L-W = 1$ ) are plotted on the pressure traces and pressure differential curves, as shown in Figure 5. When determining the IDT, ignition timing is usually defined as the instant of maximum  $dp/dt$ . While the instants of  $L-W = 1$  do not occur where the pressure rises violently but at places where chemical heat release counteracts the heat loss and the pressure begins to rise. Correspondingly,  $L-W = 1$  occurs at points where  $0 < dp/dt < 1$  in the differential curves, as shown in Figure 5b. In the L–W integral method, ignition is defined as the moment where the ignition carrier reaches its critical concentration. While in the constant volume reactor, the ignition carrier has already gone beyond its critical concentration at the instants of maximum  $dp/dt$  due to the feedback of the violent chemical heat release. Therefore, ignition predicted by the L–W integral should always be earlier than that determined by maximum  $dp/dt$  in the constant volume reactor.

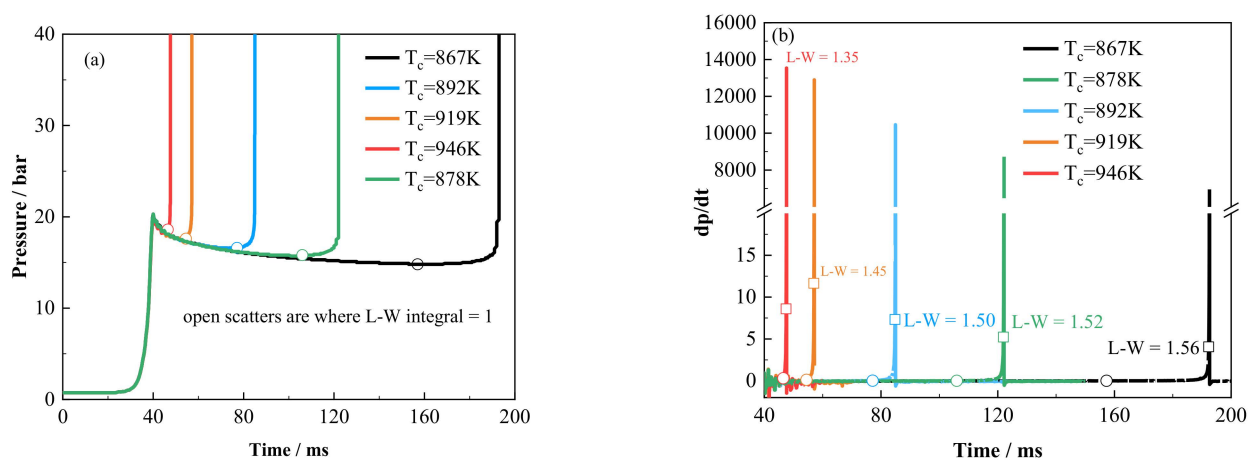


**Figure 5.** The instants of the L–W integral equal to 1 for Inputs-3. (a) The pressure profiles and (b) the differential pressure profiles of Inputs-3 from 867 K to 946 K.

### 3.2. Sensitivity of the Correlation Parameters

To obtain the IDT correlation, three parameters of the Arrhenius expression need to be optimized. Except for the initial guess, the GP model also requires a proper varying range of the parameters. Therefore, sensitivity analyses of these parameters on the IDTs were conducted, as shown in Figure 6.

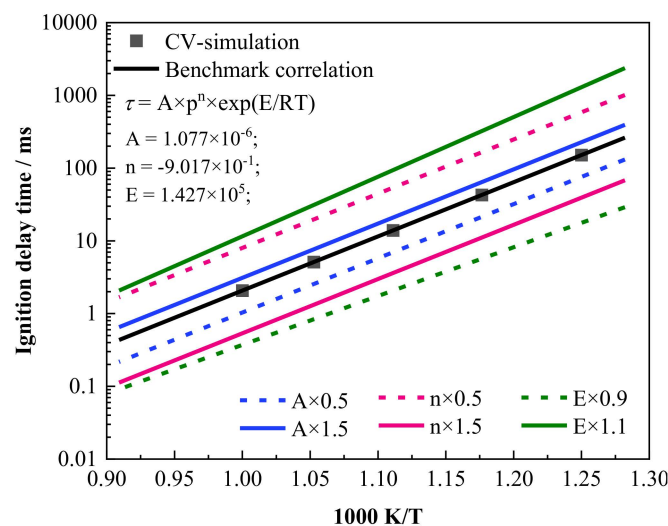


**Figure 6.** IDTs of the Arrhenius expression with varying parameter values.

The parameter  $E$  exhibits the highest sensitivity to the IDT. With only 10% variation of  $E$ , the IDTs change even more than varying  $A$  and  $n$  by 50%. A sensitivity factor,  $S$ , is calculated as defined by Equation (9).

$$S = \log(\tau_{Ri}/\tau_{Rd}) / \log(Ri/Rd) \quad (9)$$

where  $\tau_{Ri}$  is the IDT with a parameter that increases by a factor of  $Ri$ ,  $\tau_{Rd}$  is the IDT with a parameter that decreases by a factor of  $Rd$ . Physically,  $S$  indicates the order of magnitude change on IDT resulting from one order of magnitude change of the parameter. At 800 K, the  $S$  for  $A$ ,  $n$  and  $E$  are 1.0,  $-2.5$  and  $21.2$ , respectively.

The initial estimates of  $A$ ,  $n$  and  $E$ , fitted from the IDTs <sub>$f$</sub> , are listed in Table 2. The parameter  $A$  has a wide range of distribution, ranging from  $10^{-17}$  to  $10^{-6}$ . Since  $A$  shows the lowest  $S$ , a relatively wide range of  $(0$  to  $1.0 \times 10^{-5})$  was given to  $A$  during the optimization. IDT generally shows a negative correlation with pressure, so  $n$  should be negative. The changing scope of  $n$  is given as  $(-15.0$  to  $0.0)$ .

**Table 2.** Initial estimations of  $A$ ,  $n$  and  $E$  for inputs-1 to inputs-3.

Inputs	$A_0$	$n_0$	$E_0$
Inputs-1	$2.158 \times 10^{-17}$	$-10.988$	$5.6441 \times 10^5$
Inputs-2	$2.183 \times 10^{-6}$	$-3.814$	$2.0250 \times 10^5$
Inputs-3	$1.688 \times 10^{-9}$	$-5.737$	$3.0575 \times 10^5$

The parameter  $E$  corresponds to the slope of the IDT line in the log plots versus  $1000/T$ , and the optimized  $E$  should always be smaller than  $E_0$ . Therefore,  $E$  is given the scope of  $(1.0 \times 10^5$  to  $5.6 \times 10^5)$  during the optimization. Since  $E$  shows the highest  $S$ , its varying range could be gradually narrowed down based on the previous best solution during the optimization. For example, if a positive  $\delta$  is achieved at the high temperature limit and a negative  $\delta$  is achieved at the low temperature limit, respectively, the current correlation is overestimating the slope ( $E$ ). In the next cycle of optimization, current  $E$  is set as the upper limit of its varying scope.

### 3.3. IDT Correlation Using the Inverse L–W Integral Method

#### 3.3.1. Effect of Residuals on the IDT Correlation

The optimization algorithm minimizes the objective function within the specified ranges of the parameters, reducing the levels of  $\delta$  to the  $\delta_i$ . For each set of input profiles,  $\delta$  at different temperatures is averaged ( $\bar{\delta}$ ) to quantify the overall residual of the current correlation. Correlations of inputs-1 with  $\bar{\delta}$  ranging from  $-0.20$  to  $1.00$  are compared in Figure 7. Detailed values of the parameters and the corresponding  $\bar{\delta}$  are provided in the Supplementary Materials.

The adiabatic constant volume simulation result is used as the benchmark of the IDT correlation, as shown by the solid black line in Figure 7. As  $\bar{\delta}$  increases from  $-0.200$  to  $-0.025$ , the correlation becomes closer to the benchmark. However, the closest correlation is that with  $\bar{\delta} = 0.260$  rather than that with  $\bar{\delta} = 0.000$ . This is also because the L–W = 1 occurs earlier than the maximum  $dp/dt$  in the constant volume reactor, as discussed in Section 3.1. Specifically, for inputs-1, the L–W integrals at the moments of the maximum  $dp/dt$  are 1.56, 1.52, 1.50, 1.45 and 1.35 at 867 K, 878 K, 892 K, 919 K and 946 K, respectively. Consequently, inputs-1 achieves the lowest ARD at  $\bar{\delta} = 0.5$ , as shown in Figure 8. When  $\bar{\delta}$  is further increased to 1.000, the correlation has gone below the benchmark, underestimating the IDT.

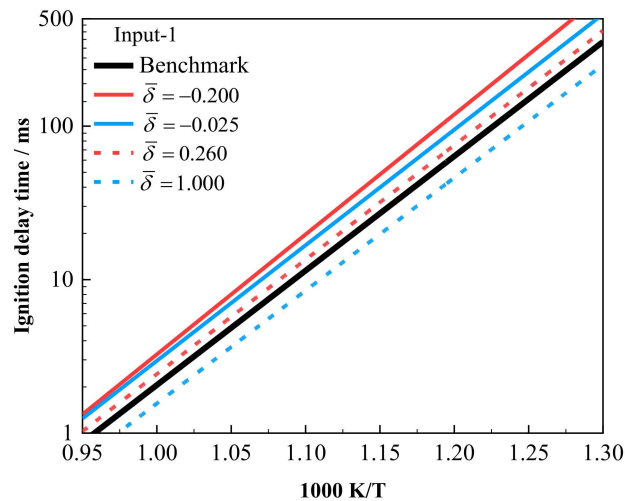


Figure 7. Correlations of inputs-1 with  $\bar{\delta}$  ranging from  $-0.200$  to  $1.000$ .

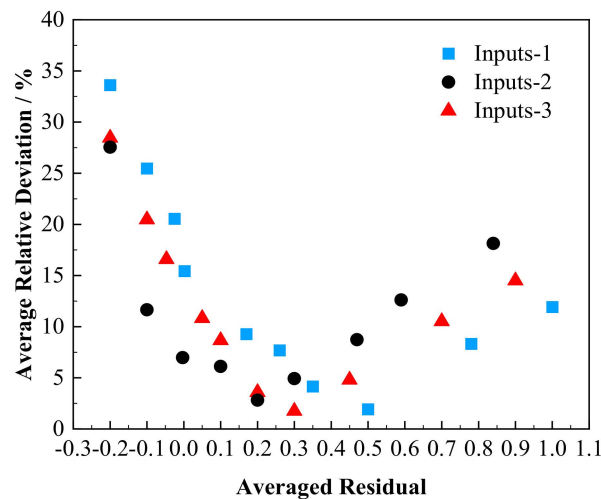


Figure 8. Effects of the averaged residual on the correlation ARD for different inputs.

The ARD of the correlations for the other inputs also shows a similar trend to that of inputs-1, as shown in Figure 8. The best residuals are all larger than 0 and are close to the value of (forward L–W integral at the instant of maximum  $dp/dt - 1$ ). This indicates that the inverse usage of the L–W integral method does not introduce extra errors, except for the errors in the forward L–W integral method itself, and by setting a proper  $\delta_t$ , the errors of the IDT correlation can be counteracted by the inherent forward L–W integral errors.

### 3.3.2. Standardization Performance of the Correlation

After obtaining the correlation, the  $IDTs_f$  can then be standardized, as shown in Figure 9. The  $IDTs_f$  of different inputs, which showed large deviation due to the facility effects, are now in good agreement after standardization, at least within the typical experimental uncertainty ( $<20\%$ ). The standardization procedure facilitates the direct comparison of the IDTs measured among different RCM facilities.

Note that the minimum absolute value of  $\bar{\delta}$  does not guarantee the highest standardization accuracy in the current algorithm, as shown in Figure 9a,b. The  $IDT_{s_{cv}}$  with the minimum absolute  $\bar{\delta}$  are higher than the benchmark by about 30% to 40%, but they exhibit the best consistency. Details of the parameter values and the corresponding  $\bar{\delta}$  for each input set are provided in Table 3.  $IDT_{s_{cv}}$ , with  $\bar{\delta} = 0.5$ , are generally lower than the benchmark

by about 20%. At  $\bar{\delta} = 0.2$ , as shown in Figure 9a, the IDTs<sub>cv</sub> agree well with the benchmark line, allowing for the direct simulation using a simple constant volume reactor.

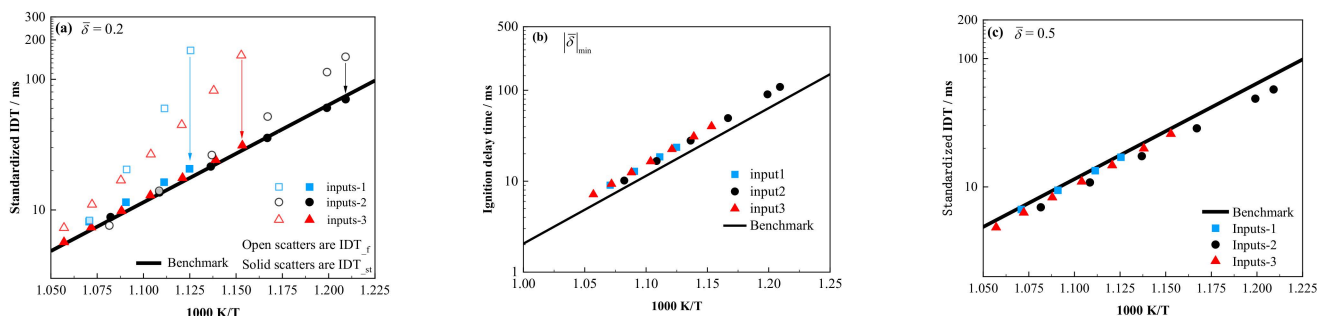


Figure 9. Standardized IDTs using correlations with different  $\bar{\delta}$ .

Table 3. Parameters with the minimum absolute value of  $\bar{\delta}$  for inputs-1 to -3.

Inputs	$ \bar{\delta} _{\min}$	A	n	$E/J \cdot \text{mol}^{-1} \cdot \text{K}^{-1}$
1	0.0020	$2.4049 \times 10^{-6}$	-1.2924	$1.4763 \times 10^5$
2	0.0004	$5.0685 \times 10^{-6}$	-1.9038	$1.5529 \times 10^5$
3	0.0470	$2.7358 \times 10^{-6}$	-1.3808	$1.4876 \times 10^5$

The standardization accuracy is dependent on  $\bar{\delta}$ , but a proper value of  $\bar{\delta}$  is unknown in practical RCM data correlation. Based on the current calculations,  $\bar{\delta}$  is suggested to be positive and would not be larger than 0.5. As shown in Figure 9c, the accuracy of the standardization deteriorates when  $\bar{\delta}$  becomes larger than 0.5. For general applications of this standardization procedure, determining a proper  $\bar{\delta}$  and feeding it back into the optimization process ( $\delta_t$ ) are needed in future works.

### 3.4. Limitation and Future Direction

Due to the simple Arrhenius IDT correlation, this standardization algorithm can currently only be applied to fuels exhibiting single-stage ignition characteristics, such as methanol, ethanol, methane, ethane and hydrogen. However, this inverse application of the L–W integral method has shown its potential for expansion to more complex fuels with two-stage ignition and NTC behaviors. As demonstrated by Pan et al. [28] and Tao [40] et al., a staged L–W integral can successfully predict the two-stage ignition behavior of the primary reference fuels. Therefore, updating the simple Arrhenius IDT correlation to a multi-stage form could enable the algorithm to accommodate larger molecular fuels.

## 4. Conclusions

This paper proposes a standardization algorithm for IDT measurements from RCMs. By applying the Livengood–Wu integral method inversely and using a Bayesian approach to optimize the correlation parameters, the IDTs, which are influenced by distinct facility effects, can be effectively correlated to those under adiabatic and constant volume conditions.

The autoignitions of an ethanol mixture under distinct facility effects were set as an example to test this algorithm. The results show that moments where the L–W = 1 generally occur earlier than the ignition defined by the maximum dp/dt due to the violent chemical heat release, and with a greater extent of heat loss in the input profile, the deviation between L–W = 1 and the maximum dp/dt increases. However, the errors of IDT<sub>cv</sub> correlation can be counteracted by the inherent forward L–W integral errors. Consequently, the IDT<sub>cv</sub> correlation achieves the highest accuracy when the algorithm takes into account this integral deviation, resulting in a relative error of less than 5%.

Although the correlation accuracy varies at different residual levels, the dispersed IDTs under facility effects can be standardized within 20% across a wide range of the algorithm residual (0.0–0.2). By applying this algorithm to the raw measurements from different RCMs, IDTs can then be directly compared without importing complex chemical kinetic modeling, thereby facilitating the assessment of the reliability of the experimental data.

**Supplementary Materials:** The following supporting information can be downloaded at: <https://www.mdpi.com/article/10.3390/en18010165/s1>, Table S1. Detailed values of the parameters and the corresponding  $\bar{\delta}$  of Inputs-1. Table S2. Detailed values of the parameters and the corresponding  $\bar{\delta}$  of Inputs-2. Table S3. Detailed values of the parameters and the corresponding  $\bar{\delta}$  of Inputs-3.

**Author Contributions:** Conceptualization, Y.W.; Validation, Z.Z.; Data curation, Z.Z.; Writing—original draft, Y.W.; Visualization, Z.Z.; Supervision, Y.W.; Funding acquisition, Y.W. All authors have read and agreed to the published version of the manuscript.

**Funding:** This work was supported by the Chongqing Key Laboratory of Fire and Explosion Safety (The Evaluating Laboratory of Military Oil Depot Safety And Facility Equipment) and the National Natural Science Foundation of China (52206168).

**Data Availability Statement:** The original contributions presented in this study are included in the article/supplementary material. Further inquiries can be directed to the corresponding author.

**Conflicts of Interest:** The authors declare that they have no known competing financial interests or personal relationships that could have appeared to influence the work reported in this paper.

## References

1. Shi, Z.; Lee, C.-F.; Wu, H.; Wu, Y.; Zhang, L.; Liu, F. Optical diagnostics of low-temperature ignition and combustion characteristics of diesel/kerosene blends under cold-start conditions. *Appl. Energy* **2019**, *251*, 113307. [CrossRef]
2. Topgül, T.; Yücesu, H.S.; Çinar, C.; Koca, A. The effects of ethanol–unleaded gasoline blends and ignition timing on engine performance and exhaust emissions. *Renew. Energy* **2006**, *31*, 2534–2542. [CrossRef]
3. Bednarski, M.; Orliński, P.; Wojs, M.K.; Sikora, M. Evaluation of methods for determining the combustion ignition delay in a diesel engine powered by liquid biofuel. *J. Energy Inst.* **2019**, *92*, 1107–1114. [CrossRef]
4. Goldsborough, S.S.; Hochgreb, S.; Vanhove, G.; Wooldridge, M.S.; Curran, H.J.; Sung, C.-J. Advances in rapid compression machine studies of low- and intermediate-temperature autoignition phenomena. *Prog. Energy Combust. Sci.* **2017**, *63*, 1–78. [CrossRef]
5. Reyes, M.; Tinaut, F.V.; Andrés, C.; Pérez, A. A method to determine ignition delay times for Diesel surrogate fuels from combustion in a constant volume bomb: Inverse Livengood–Wu method. *Fuel* **2012**, *102*, 289–298. [CrossRef]
6. Wu, H.; Sun, W.; Huang, Z.; Zhang, Y. Biphasic sensitization effect of NO<sub>2</sub> on n-C<sub>4</sub>H<sub>10</sub> auto-ignition. *Combust. Flame* **2022**, *237*, 111844. [CrossRef]
7. Lisochkin, Y.A.; Malakhov, K.V.; Poznyak, V.I. Global Kinetic Parameters for Determining the Autoignition Limits and Induction Periods for Mixtures of Methane, Ammonia, Oxygen, and Nitrogen, Combustion. *Explos. Shock Waves* **2004**, *40*, 253–257. [CrossRef]
8. Atef, N.; Kukkadapu, G.; Mohamed, S.Y.; Rashidi, M.A.; Banyon, C.; Mehl, M.; Heufer, K.A.; Nasir, E.F.; Alfazazi, A.; Das, A.K.; et al. A comprehensive iso-octane combustion model with improved thermochemistry and chemical kinetics. *Combust. Flame* **2017**, *178*, 111–134. [CrossRef]
9. Preußker, M.; Büttgen, R.D.; Noé, M.R.; Heufer, K.A. Finding a common ground for RCM experiments. Part A: On the influences of facility effects regarding the reliability of experimental validations. *Combust. Flame* **2024**, *262*, 113323. [CrossRef]
10. Sun, W.; Huang, W.; Qin, X.; Deng, Y.; Kang, Y.; Peng, W.; Zhang, Y.; Huang, Z. Water impact on the auto-ignition of kerosene/air mixtures under combustor relevant conditions. *Fuel* **2020**, *267*, 117184. [CrossRef]
11. Wu, Y.; Tang, C.; Yang, M.; Wang, Q.-D.; Huang, Z.; Zhao, P.; Curran, H.J. Evaluation of non-ideal piston stopping effects on the “adiabatic core” and ignition delay time simulation in rapid compression machines. *Combust. Flame* **2020**, *218*, 229–233. [CrossRef]
12. Büttgen, R.D.; Preußker, M.; Kang, D.; Cheng, S.; Goldsborough, S.S.; Issayev, G.; Farooq, A.; Song, H.; Fenard, Y.; Vanhove, G.; et al. Finding a common ground for RCM experiments. Part B: Benchmark study on ethanol ignition. *Combust. Flame* **2024**, *262*, 113338. [CrossRef]

13. Wu, Y.; Kong, X.; Ao, Y.; Hou, Y.; Wang, J.; Yin, G.; Sun, W.; Zhang, Y.; Huang, Z.; Tang, C. Experimental and kinetic modeling study on the low-temperature decomposition and autoignition of 2-Azido-N,N-dimethylethanamine: A promising green mono- and bi-propellant. *Proc. Combust. Inst.* **2024**, *40*, 105359. [[CrossRef](#)]
14. Wu, Y.; Yang, M.; Yao, X.; Liu, Y.; Tang, C. Comparative studies on the ignition characteristics of diisobutylene isomers and iso-octane by using a rapid compression machine. *Fuel* **2020**, *276*, 118008. [[CrossRef](#)]
15. Sarathy, S.M.; Park, S.; Weber, B.W.; Wang, W.; Veloo, P.S.; Davis, A.C.; Togbe, C.; Westbrook, C.K.; Park, O.; Dayma, G.; et al. A comprehensive experimental and modeling study of iso-pentanol combustion. *Combust. Flame* **2013**, *160*, 2712–2728. [[CrossRef](#)]
16. Weber, B.W.; Sung, C.-J. Comparative Autoignition Trends in Butanol Isomers at Elevated Pressure. *Energy Fuels* **2013**, *27*, 1688–1698. [[CrossRef](#)]
17. Wu, Y.; Yang, M.; Tang, C.; Liu, Y.; Zhang, P.; Huang, Z. Promoting “adiabatic core” approximation in a rapid compression machine by an optimized creviced piston design. *Fuel* **2019**, *251*, 328–340. [[CrossRef](#)]
18. Livengood, J.C.; Wu, P.C. Correlation of autoignition phenomena in internal combustion engines and rapid compression machines. *Symp. (Int.) Combust.* **1955**, *5*, 347–356. [[CrossRef](#)]
19. Song, H.; Song, H.H. Correlated ignition delay expression of two-stage ignition fuels for Livengood–Wu model-based knock prediction. *Fuel* **2020**, *260*, 116404. [[CrossRef](#)]
20. Yue, Z.; Xu, C.; Som, S.; Sluder, C.S.; Edwards, K.D.; Whitesides, R.A.; McNenly, M.J. A Transported Livengood–Wu Integral Model for Knock Prediction in Computational Fluid Dynamics Simulation. *J. Eng. Gas Turbines Power* **2021**, *143*, 091017. [[CrossRef](#)]
21. Ji, F.; Meng, S.; Han, Z. Knock Prediction Improvement with Application to the Analysis of Knock Mitigation with Targeted Water Injection in SI Engines. *Combust. Sci. Technology* **2024**, 1–29. [[CrossRef](#)]
22. Ji, F.; Meng, S.; Han, Z.; Dong, G.; Reitz, R.D. Progress in knock combustion modeling of spark ignition engines. *Appl. Energy* **2025**, *378*, 124852. [[CrossRef](#)]
23. Ebrahimi, K.; Patidar, L.; Koutsivitis, P.; Fogla, N.; Wahiduzzaman, S. Machine Learning Tabulation Scheme for Fast Chemical Kinetics Computation. *Sae Int. J. Engines* **2024**, *17*, 477–492. [[CrossRef](#)]
24. Rrustemi, D.N.; Ganippa, L.C.; Axon, C.J. Investigation of boost pressure and spark timing on combustion and NO emissions under lean mixture operation in hydrogen engines. *Fuel* **2023**, *353*, 129192. [[CrossRef](#)]
25. Hernández, J.J.; Lapuerta, M.; Sanz-Argent, J. Autoignition prediction capability of the Livengood–Wu correlation applied to fuels of commercial interest. *Int. J. Engine Res.* **2014**, *15*, 817–829. [[CrossRef](#)]
26. Khaled, F.; Javed, T.; Farooq, A.; Badra, J. Analysis of ignition temperature range and surrogate fuel requirements for GCI engine. *Fuel* **2022**, *312*, 122978. [[CrossRef](#)]
27. Khaled, F.; Badra, J.; Farooq, A. Ignition delay time correlation of fuel blends based on Livengood–Wu description. *Fuel* **2017**, *209*, 776–786. [[CrossRef](#)]
28. Pan, J.; Zhao, P.; Law, C.K.; Wei, H. A predictive Livengood–Wu correlation for two-stage ignition. *Int. J. Engine Res.* **2016**, *17*, 825–835. [[CrossRef](#)]
29. Miyoshi, A. Kinetics of autoignition: A simple intuitive interpretation and its relation to the Livengood–Wu integral. *Phys. Chem. Chem. Phys.* **2018**, *20*, 10762–10769. [[CrossRef](#)]
30. Tao, M.; Laich, A.; Lynch, P.; Zhao, P. On the Interpretation and Correlation of High-Temperature Ignition Delays in Reactors with Varying Thermodynamic Conditions. *Int. J. Chem. Kinet.* **2018**, *50*, 410–424. [[CrossRef](#)]
31. Zhang, K.; Banyon, C.; Bugler, J.; Curran, H.J.; Rodriguez, A.; Herbinet, O.; Battin-Leclerc, F.; B’Chir, C.; Heufer, K.A. An updated experimental and kinetic modeling study of n-heptane oxidation. *Combust. Flame* **2016**, *172*, 116–135. [[CrossRef](#)]
32. Shah, A.; Cheng, S.; Longman, D.E.; Goldsborough, S.S.; Rockstroh, T. An experimental study of uncertainty considerations associated with predicting auto-ignition timing using the Livengood–Wu integral method. *Fuel* **2021**, *286*, 119025. [[CrossRef](#)]
33. Wu, Y.; Kong, X.; Yu, T.; Mai, Z.; Cao, S.; Yu, Q.; Liang, J.; Nagaraja, S.S.; Sarathy, S.M.; Huang, Z.; et al. Experimental and kinetic modeling study of tetramethylethylenediamine: A promising green propellant fuel. *Combust. Flame* **2023**, *248*, 112584. [[CrossRef](#)]
34. Wu, Y.; Panigrahy, S.; Sahu, A.B.; Bariki, C.; Beeckmann, J.; Liang, J.; Mohamed, A.A.E.; Dong, S.; Tang, C.; Pitsch, H.; et al. Understanding the antagonistic effect of methanol as a component in surrogate fuel models: A case study of methanol/n-heptane mixtures. *Combust. Flame* **2021**, *226*, 229–242. [[CrossRef](#)]
35. Zhang, Y.; El-Merhubi, H.; Lefort, B.; Le Moyne, L.; Curran, H.J.; Kéromnès, A. Probing the low-temperature chemistry of ethanol via the addition of dimethyl ether. *Combust. Flame* **2018**, *190*, 74–86. [[CrossRef](#)]
36. Mittal, G.; Burke, S.M.; Davies, V.A.; Parajuli, B.; Metcalfe, W.K.; Curran, H.J. Autoignition of ethanol in a rapid compression machine. *Combust. Flame* **2014**, *161*, 1164–1171. [[CrossRef](#)]
37. Leplat, N.; Dagaut, P.; Togbé, C.; Vandooren, J. Numerical and experimental study of ethanol combustion and oxidation in laminar premixed flames and in jet-stirred reactor. *Combust. Flame* **2011**, *158*, 705–725. [[CrossRef](#)]
38. Veloo, P.S.; Wang, Y.L.; Egolfopoulos, F.N.; Westbrook, C.K. A comparative experimental and computational study of methanol, ethanol, and n-butanol flames. *Combust. Flame* **2010**, *157*, 1989–2004. [[CrossRef](#)]

39. Liu, P. (Ed.) Bayesian Optimization Overview. In *Bayesian Optimization: Theory and Practice Using Python*; Apress: Berkeley, CA, USA, 2023; pp. 1–32.
40. Tao, M.; Han, D.; Zhao, P. An alternative approach to accommodate detailed ignition chemistry in combustion simulation. *Combust. Flame* **2017**, *176*, 400–408. [[CrossRef](#)]

**Disclaimer/Publisher’s Note:** The statements, opinions and data contained in all publications are solely those of the individual author(s) and contributor(s) and not of MDPI and/or the editor(s). MDPI and/or the editor(s) disclaim responsibility for any injury to people or property resulting from any ideas, methods, instructions or products referred to in the content.